

Neutrino Transport in Strongly Magnetized Proto-Neutron Stars and the Origin of Pulsar Kicks: The Effect of Asymmetric Magnetic Field Topology

Dong Lai

Department of Astronomy, Space Sciences Building, Cornell University, Ithaca, NY 14853

E-mail: dong@spacenet.tn.cornell.edu

and

Yong-Zhong Qian

Physics Department, 161-33, California Institute of Technology, Pasadena, CA 91125

ABSTRACT

In proto-neutron stars with strong magnetic fields, the cross section for ν_e ($\bar{\nu}_e$) absorption on neutrons (protons) depends on the local magnetic field strength due to the quantization of energy levels for the e^- (e^+) produced in the final state. If the neutron star possesses an asymmetric magnetic field topology in the sense that the magnitude of magnetic field in the north pole is different from that in the south pole, then asymmetric neutrino emission may be generated. We calculate the absorption cross sections of ν_e and $\bar{\nu}_e$ in strong magnetic fields as a function of the neutrino energy. These cross sections exhibit oscillatory behaviors which occur because new Landau levels for the e^- (e^+) become accessible as the neutrino energy increases. By evaluating the appropriately averaged neutrino opacities, we demonstrate that the change in the local neutrino flux due to the modified opacities is rather small. To generate appreciable kick velocity ($\sim 300 \text{ km s}^{-1}$) to the newly-formed neutron star, the difference in the field strengths at the two opposite poles of the star must be at least 10^{16} G . We also consider the magnetic field effect on the spectral neutrino energy fluxes. The oscillatory features in the absorption opacities give rise to modulations in the emergent spectra of ν_e and $\bar{\nu}_e$.

Subject headings: stars: neutron – pulsars: general – supernovae: general – dense matter – magnetic fields – radiation transfer

1. Introduction

It has been recognized shortly after the discovery of pulsars that neutron stars have velocities much in excess of those of any other normal stellar populations in our Galaxy (Gunn & Ostriker

1970; Minkowski 1970). However, it is only in the last few years that a significant body of evidence has come into place to support the view that type II supernovae are nonspherical and neutron stars receive large kick velocities at birth. Lyne and Lorimer (1994) analyzed pulsar velocities in light of new proper-motion measurements (Harrison et al. 1993) and up-to-date pulsar distance scale (Taylor & Cordes 1993), and concluded that pulsars were born with a mean speed of $\sim 450 \text{ km s}^{-1}$, much larger than previously thought. More recent studies of pulsar velocities have adopted more sophisticated statistical methods and included better treatment of selection effects and uncertainties (Lorimer et al. 1997; Hansen & Phinney 1997; Cordes & Chernoff 1997). They all yielded a result for the pulsar birth velocity in qualitative agreement (although not in quantitative details) with that of Lyne & Lorimer (1994). In particular, Cordes and Chernoff (1997) found that the three-dimensional space velocities of their sample of 47 pulsars have a bimodal distribution, with characteristic speeds of 180 km s^{-1} and 700 km s^{-1} (corresponding to 80% and 20% of the population). They also estimated that pulsars with velocities greater than 1000 km s^{-1} may be underrepresented owing to selection effects in pulsar surveys [The uncertainty in the high-velocity end of the pulsar velocity distribution function has also been emphasized by Hansen & Phinney (1997)]. Concrete evidence for the existence of pulsars with velocities of $\gtrsim 1000 \text{ km s}^{-1}$ has come from the observation of the Guitar Nebula pulsar (B2224+65), which produces a bow shock when plowing through the interstellar medium (Cordes, Romani & Lundgren 1993). In addition, studies of pulsar-supernova remnant associations have uncovered a number of pulsars having velocities much greater than 1000 km s^{-1} (Frail et al. 1994), although in many cases the associations are not completely secure.

Compelling evidence for supernova asymmetry and pulsar kicks also comes from the detection of geodetic precession in the binary pulsar PSR 1913+16 (Cordes et al. 1990; Arzoumanian et al. 1996), and the orbital plane precession in the PSR J0045-7319/B star binary (Lai et al. 1995; Kaspi et al. 1996) and its fast orbital decay (which indicates retrograde rotation of the B star with respect to the orbit; see Lai 1996). These results demonstrate that binary break-up (as originally suggested by Gott, Gunn & Ostriker 1970; see Iben & Tutukov 1996) can not be *solely* responsible for the observed pulsar velocities, and that *natal kicks are required*. In addition, evolutionary studies of neutron star binary population imply the existence of pulsar kicks (e.g., Deway & Cordes 1987; Fryer & Kalogera 1997; Fryer et al. 1998; see also Brandt & Podsiadlowski 1995). Finally, there are a large number of direct observations of nearby supernovae (e.g., Cropper et al. 1988; Trammell et al. 1993; McCray 1993; Utrobin et al. 1995) and supernova remnants (e.g., Morse, Winkler & Kirshner 1995; Aschenbach et al. 1995) in radio, optical, and X-ray bands which support the notion that supernova explosions are not spherically symmetric.

The origin of the pulsar velocities is still unknown. Two classes of mechanisms for the *natal kicks* have been suggested¹. The first class relies on convective instabilities in the collapsed stellar

¹These exclude the slow, post-explosion rocket effect due to electromagnetic radiation from off-centered magnetic dipole moment (Harrison & Tademaru 1975).

core and within the rebounding shock (e.g., Burrows & Fryxell 1992; Burrows et al. 1995; Janka & Müller 1994, 1996; Herant et al. 1994). The asymmetries in the matter and temperature distributions associated with the instabilities naturally lead to asymmetric matter ejection and/or asymmetric neutrino emission. Numerical simulations indicate that the local, post-collapse instabilities are not adequate to account for kick velocities higher than a few hundred km s^{-1} (Janka & Müller 1994). A variant of this class of models therefore relies on the global asymmetric perturbations seeded in the presupernova cores (Goldreich et al. 1996; see also Bazan & Arnett 1994). Clearly, the magnitude of kick velocity depends on the degree of initial asymmetry in the imploding core (Burrows & Hayes 1996). Due to various uncertainties in the presupernova stellar models, it is not clear at this point whether sufficiently large initial perturbations can be produced in the precollapse core (Lai & Goldreich 1998).

In this paper we focus on the second class of models in which the large pulsar kick velocities arise from asymmetric neutrino emission induced by strong magnetic fields. Since 99% of the neutron star binding energy (a few times 10^{53} erg) is released in neutrinos, tapping the neutrino energy would appear to be an efficient means to kick the newly-formed neutron star. Magnetic fields are naturally invoked to break the spherical symmetry in neutrino emission. But the actual mechanism is unclear. We first briefly comment on previous works on this and related subjects.

1.1. Previous Works on Asymmetric Neutrino Emission Induced by Magnetic Fields

A number of authors have noted that parity violation in weak interactions may lead to asymmetric neutrino emission from proto-neutron stars (Chugai 1984; Dorofeev et al. 1985; Vilenkin 1995; Horowitz & Piekarewicz 1997). However, their studies are largely unsatisfactory for a number of reasons: they either failed to identify the most relevant neutrino emission/interaction processes or the relevant physical conditions in proto-neutron stars, or stopped at estimating the magnetic field effects on neutrino opacities. Chugai (1984) and Vilenkin (1995) (see also Bezchastnov & Haensel 1996) considered neutrino-electron scattering and concluded that the effect is extremely small² (e.g., to obtain $V_{\text{kick}} = 300 \text{ km s}^{-1}$ would require a magnetic field of at least 10^{16} G). However, neutrino-electron scattering is less important than neutrino-nucleon scattering in determining the characteristics of neutrino transport in proto-neutron stars. Similarly, Dorofeev et al. (1985) considered neutrino emission by Urca processes in strong magnetic fields. But as shown by Lai & Qian (1998), in the bulk interior of the neutron star, the asymmetry associated with neutrino emission is cancelled by the asymmetry associated with neutrino absorption.

Concerning the parity violation effect in proto-neutron stars, Horowitz & Li (1997) recently suggested that the asymmetry in neutrino emission may be enhanced due to multiple scatterings

²Note that Chugai’s estimate for the electron polarization in the relativistic and degenerate regime (the relevant physical regime) is incorrect. This error leads to an overestimate of the effect as compared to Vilenkin’s result.

of neutrinos by nucleons which are slightly polarized by the magnetic field. They estimated that a field strength of a few times 10^{12} G is adequate to account for kick velocities of a few hundred km s^{-1} . However, the paper by Horowitz & Li (1997) only discusses the idealized situations of scattering media, and ignores various essential physics that is needed in a proper treatment of neutrino transport in proto-neutron stars. In particular, it does not consider the effect of neutrino absorption which one might suspect to wash out the cumulative effect from multiple scatterings. Our own study of the parity violation effect (Lai & Qian 1998) was flawed in the treatment of scattering terms in the neutrino transport equation. As shown by Arras & Lai (1998), detailed balance requires that there be no cumulative effect from multiple scatterings in the bulk interior of the proto-neutron star where local thermodynamic equilibrium applies to a good approximation. Enhancement of neutrino emission asymmetry from multiple scatterings obtains only after neutrinos thermally decouple from proto-neutron star matter, and therefore is insignificant.

Bisnovatyi-Kogan (1993) attributed pulsar kicks to asymmetric magnetic field distribution in proto-neutron stars. Using the fact that neutron decay rate can be modified by the magnetic field, he inferred that neutrino emissions from opposite sides of the neutron star surface are different. However, neutron decay is not directly relevant for neutrino emission from a newly-formed neutron star. Roulet (1997) (whose paper was posted while this paper was being written) considered the relevant neutrino absorption processes. But his study was restricted to calculating the neutrino cross sections as functions of neutrino energy (corresponding to §2.1 of this paper), and therefore was insufficient for addressing the issue of asymmetric neutrino emission.

Finally, it is worthwhile to mention a speculative idea on pulsar kicks which relies on nonstandard neutrino physics. Kusenko & Segrè (1996) suggested that asymmetric ν_τ emission could result from the Mikheyev-Smirnov-Wolfenstein flavor transformation between ν_τ and ν_e inside a magnetized proto-neutron star because a magnetic field changes the resonance condition for the flavor transformation. With a ν_τ mass of ~ 100 eV, they claimed that magnetic fields of $\sim 3 \times 10^{14}$ G can give the pulsar a kick velocity of a few hundred km s^{-1} . However, their treatment of neutrino transport was oversimplified: e.g., they ignored that neutrinos of different energies have different resonance surfaces. Furthermore, a simple geometric effect and realistic proto-neutron star conditions easily reduce their estimated kick velocity by an order of magnitude. Most likely, a magnetic field strength of $\sim 10^{16}$ G is needed to produce the observed average pulsar kick velocity via their mechanism (see Qian 1997). Similarly strong magnetic fields are required in variants of the Kusenko & Segrè mechanism, e.g., those considered by Akhmedov et al. (1997) (which relies on both the neutrino mass and the neutrino magnetic moment to facilitate the flavor transformation).

1.2. Plan of This Paper

As should be clear from the brief review in §1.1, in spite of quite a number of suggestions, there is at present no consensus on the magnitudes of the magnetic field induced asymmetry in

neutrino emission from proto-neutron stars and the resulting kick velocities. In this paper we study the effect of asymmetric magnetic field topology on pulsar kicks. Since the energy levels of e^- and e^+ in a magnetic field are quantized, the ν_e and $\bar{\nu}_e$ absorption opacities near the neutrinosphere and the neutrino-matter decoupling region depend on the local magnetic field strength. If the *magnitude* of magnetic field in the north pole is different from that in the south pole (the field does not need to be ordered), then asymmetric neutrino flux may be generated. Here we ignore the effects of magnetic fields on the proto-neutron star structure through the equation of state — these are secondary effects as far as neutrino transport is concerned.

The organization of this paper is as follows. In §2 we calculate the ν_e and $\bar{\nu}_e$ absorption cross sections as functions of neutrino energy in strong magnetic fields. Section 3 summarizes the basic features of neutrino transport near the neutron star surface. In §4 we derive and evaluate the “Rosseland mean” neutrino opacities which are directly related to the local neutrino flux. We then consider in §5 the change in neutrino flux due to the modified opacities, and estimate the kick velocity resulting from an asymmetric magnetic field topology. In §6 we briefly consider how the emergent neutrino spectra may be modified by the strong magnetic field. In §7 we present our conclusion.

Unless noted otherwise, we shall use units in which \hbar , c , and the Boltzmann constant k are unity.

2. ν_e and $\bar{\nu}_e$ Absorption Cross Sections in Strong Magnetic Fields

In this section we consider how magnetic fields modify the (total) neutrino absorption ($\nu_e + n \rightarrow p + e^-$ and $\bar{\nu}_e + p \rightarrow n + e^+$) cross sections for specific neutrino energies. We present our calculation of the ν_e absorption cross section in detail. The $\bar{\nu}_e$ absorption cross section can be obtained in a similar manner.

To begin with, it is useful to review various energy scales involved in the problem. Near the neutrinosphere and the neutrino-matter decoupling region, the matter density is typically 10^{11} – 10^{12} g cm^{-3} , and the temperature is about several MeV. The electrons are extremely relativistic and highly degenerate, with Fermi energy $E_{F,e} \simeq 51.5 (Y_e \rho_{12})^{1/3}$ MeV, where $Y_e \sim 0.1$ is the electron fraction (the number of electrons per nucleon) and $\rho_{12} = \rho / (10^{12} \text{ g cm}^{-3})$. The neutrons and protons have Fermi energies $E_{F,n} = 1.4 [(1 - Y_e) \rho_{12}]^{2/3}$ MeV and $E_{F,p} = 1.4 (Y_e \rho_{12})^{2/3}$ MeV, respectively, and thus they are essentially nondegenerate.

2.1. The Cross Sections

In strong magnetic fields the transverse motion of the electron is quantized into Landau levels. The electron energy dispersion relation is

$$E_e = \left[p_z^2 + m_e^2(1 + 2nb) \right]^{1/2}, \quad n = 0, 1, 2, \dots \quad (1)$$

where p_z is the longitudinal momentum (along the magnetic field), and n is the Landau level index. The dimensionless field strength b is defined as

$$b \equiv \frac{B}{B_c}, \quad \text{with } B_c = \frac{m_e^2 c^3}{\hbar e} = 4.414 \times 10^{13} \text{ G}. \quad (2)$$

[B_c is the critical field strength defined by equating the cyclotron energy $\hbar e B / (m_e c)$ to $m_e c^2$.] The quantization effect on the proton is extremely small due to the large proton mass, and is neglected throughout this paper.

Since the cyclotron radius (characterizing the size of the Landau wavefunction) $[\hbar c / (eB)]^{1/2} = [\hbar / (m_e c)] b^{-1/2} = 386 b^{-1/2} \text{ fm}$ is much greater than the range of the weak interaction [$\hbar / (m_W c) \simeq 2.5 \times 10^{-3} \text{ fm}$, where $m_W \simeq 80 \text{ GeV}$ is the mass of W boson], one can use the $V - A$ theory with contact interaction. Locally (at the point of interaction) the Landau wavefunction resembles a plane wave. Thus we expect that the spin-averaged matrix element is the same as in the case without magnetic fields. This expectation has been borne out by detailed calculations (e.g., Fassio-Canuto 1969; Matese & O’Connell 1969). Therefore we only need to consider the effect of magnetic field on the electron phase space.

Since the neutrino energy (a few to tens of MeV) of interest is much less than the nucleon mass, we first consider the case where the nucleon mass is taken to be infinity, an approximation adopted in the standard zero-field calculations (e.g., Tubbs & Schramm 1975). The cross section for $\nu_e + n \rightarrow p + e^-$ can be written as a sum over the (spatial and spin) states of the electron (per unit volume)

$$\sigma_B^{(\text{abs})}(E_\nu) = A \sum_e (1 - f_e) \delta(E_\nu + Q - E_e), \quad (3)$$

where we have defined

$$A \equiv \pi G_F^2 \cos^2 \theta_C (c_V^2 + 3c_A^2), \quad (4)$$

and the other symbols have their usual meanings: $G_F = (293 \text{ GeV})^{-2}$ is the universal Fermi constant, $\cos^2 \theta_C = 0.95$ refers to the Cabbibo angle, $c_V = 1$ and $c_A = 1.26$ are the coupling constants, $Q = m_n - m_p = 1.293 \text{ MeV}$ is the neutron-proton mass difference, E_ν is the ν_e energy, and $(1 - f_e)$ is the Pauli blocking factor. The electron occupation number f_e is

$$f_e = \frac{1}{\exp[(E_e - \mu_e)/T] + 1}, \quad (5)$$

where E_e is the electron energy, μ_e is the electron chemical potential, and T is the matter temperature. For zero field, the sum becomes $2 \int d^3p/(2\pi)^3$, and we have

$$\sigma_{B=0}^{(\text{abs})}(E_\nu) = \frac{A}{\pi^2}(E_\nu + Q) \left[(E_\nu + Q)^2 - m_e^2 \right]^{1/2} (1 - f_e), \quad (6)$$

with $E_e = E_\nu + Q$. For $B \neq 0$, knowing that the degeneracy of the Landau level (per unit area) is $g_n eB/hc = g_n m_e^2 b/(2\pi)$, with $g_n = 1$ for $n = 0$ and $g_n = 2$ for $n > 0$, we have

$$\sigma_B^{(\text{abs})}(E_\nu) = A \int_{-\infty}^{\infty} \frac{dp_z}{2\pi} \sum_n g_n \frac{m_e^2 b}{2\pi} (1 - f_e) \delta(E_\nu + Q - E_e) = A \frac{m_e^2 b}{2\pi^2} \sum_{n=0}^{n_{\text{max}}} g_n \frac{E_e}{p_{z,n}} (1 - f_e), \quad (7)$$

where $E_e = E_\nu + Q$, and $p_{z,n} = [E_e^2 - m_e^2(1 + 2nb)]^{1/2}$. The upper limit n_{max} for the sum is the maximum value of n for which $p_{z,n}$ is meaningfully defined, i.e.,

$$n_{\text{max}} = \text{Int} \left[\frac{(E_\nu + Q)^2 - m_e^2}{2m_e^2 b} \right], \quad (8)$$

where $\text{Int}[x]$ stands for the integral part of x . Henceforth, n_{max} is similarly defined, and we shall not explicitly write out the lower and upper limits for the sum.

Figure 1 depicts $\sigma_B^{(\text{abs})}(E_\nu)$ for $b = 100$ and $\sigma_{B=0}^{(\text{abs})}(E_\nu)$ as functions of E_ν for typical conditions ($Y_e = 0.1$, $\mu_e = 20$ MeV, and $T = 3$ MeV) in a proto-neutron star. Note that ideally, one should compare $\sigma_B^{(\text{abs})}(E_\nu)$ and $\sigma_{B=0}^{(\text{abs})}(E_\nu)$ at the same matter density. For $\mu_e \simeq E_{F,e} \gg T$ (so that $n_{e^-} \gg n_{e^+}$), the matter density is related to μ_e via

$$\rho = \frac{m_n}{Y_e} \frac{1}{\pi^2} \int_0^\infty p^2 dp f_e, \quad (\text{for } B = 0), \quad (9)$$

$$\rho = \frac{m_n}{Y_e} \frac{m_e^2 b}{2\pi^2} \int_0^\infty dp_z \sum_n g_n f_e, \quad (\text{for } B \neq 0). \quad (10)$$

In practice, we have found that for a given μ_e , the dependence of ρ on the field strength is rather weak for the range of parameters of interest in this paper. Thus in all of our calculations here and below, we compare the cross sections at a given μ_e . A prominent feature of $\sigma_B^{(\text{abs})}(E_\nu)$ shown in Fig. 1 is the presence of “resonances,” which occur when $p_{z,n} = 0$ (cf. Eq. [7]), i.e., at the neutrino energies for which the final state electron lies in a “stationary” Landau level (with zero longitudinal momentum). These resonances reflect the divergence of the density of states of electrons at these stationary Landau levels.

The cross section for $\bar{\nu}_e + p \rightarrow n + e^+$ can be similarly calculated. One only needs to replace Q with $-Q$ and μ_e with $-\mu_e$ in the expressions for ν_e absorption to obtain the desired expressions for $\bar{\nu}_e$ absorption. The numerical results for $\bar{\nu}_e$ absorption cross section are shown in Fig. 2 for the same physical parameters as used in Fig. 1.

2.2. Thermal Averaging

The divergent cross sections at the “resonances” shown in Figs. 1 and 2 are clearly unphysical. They are smoothed out by the thermal motion of the neutron. To the leading order, the width of the resonance is $(kT/m_n)^{1/2}E_\nu$, corresponding to the Doppler shift of the neutrino energy in the neutron’s rest frame. The recoil energy, of order E_ν^2/m_n , is much less effective in smoothing out the resonances, and will be neglected. With this approximation, the smoothed cross section can be written as

$$\langle \sigma_B^{(\text{abs})}(E_\nu) \rangle \simeq \frac{1}{(2\pi)^2} \int v_n^2 dv_n f_n \int d \cos \theta_n \sigma_B^{(\text{abs})}(E'_\nu), \quad (11)$$

where $E'_\nu = E_\nu(1 - v_n \cos \theta_n)$ and $f_n = (2\pi m_n/T)^{3/2} \exp(-m_n v_n^2/2T)$ is the velocity distribution function for the neutron. If we replace the factor $(1 - f_e)$ [which depends on $(E'_\nu + Q)$] in $\sigma_B^{(\text{abs})}(E'_\nu)$ with the average value $\langle 1 - f_e \rangle$, which can be approximately taken as $(1 - f_e)$ evaluated at $E_e = E_\nu + Q$, then the angular integral in Eq. (11) can be carried out analytically. For $B = 0$, we have

$$\langle \sigma_{B=0}^{(\text{abs})}(E_\nu) \rangle \simeq \frac{A}{(2\pi)^2} \langle 1 - f_e \rangle \int v_n dv_n f_n \frac{1}{3\pi^2 E_\nu} (E_e^2 - m_e^2)^{3/2} \Bigg|_{E_e=E_\nu(1-v_n)+Q}^{E_e=E_\nu(1+v_n)+Q}, \quad (12)$$

which is reduced to

$$\langle \sigma_{B=0}^{(\text{abs})}(E_\nu) \rangle \simeq \frac{A}{\pi^2} (E_\nu + Q)^2 \langle 1 - f_e \rangle \left[1 + \left(\frac{E_\nu}{E_\nu + Q} \right)^2 \frac{T}{m_n} \right] \quad (13)$$

if we neglect the electron mass m_e . For $B \neq 0$, we find³

$$\langle \sigma_B^{(\text{abs})}(E_\nu) \rangle \simeq \frac{A}{(2\pi)^2} \langle 1 - f_e \rangle \int v_n dv_n f_n \frac{m_e^2 b}{2\pi^2 E_\nu} \sum_n g_n [E_e^2 - m_e^2(1 + 2nb)]^{1/2} \Bigg|_{E_e=E_\nu(1-v_n)+Q}^{E_e=E_\nu(1+v_n)+Q}. \quad (14)$$

We could have approximately included the neutron recoil effect by replacing Q with $Q - (E_\nu + Q)^2/(2m_n)$ in Eqs. (12)–(14). But we choose to leave out this effect since as mentioned previously, it is ineffective in smoothing out the resonances in $\sigma_B^{(\text{abs})}(E_\nu)$. We have numerically evaluated Eqs. (12) and (14), and the results are depicted in Fig. 1 together with the cross sections before averaging. Similar results for the $\bar{\nu}_e$ absorption cross section are shown in Fig. 2. As expected, we find that for $B = 0$, the averaged cross section $\langle \sigma_{B=0}^{(\text{abs})}(E_\nu) \rangle$ is almost identical to $\sigma_{B=0}^{(\text{abs})}(E_\nu)$ (see Eq. [13]). However, for $B \neq 0$, the thermal averaging is essential in obtaining the smoothed physical absorption cross sections.

³To obtain this result, one has to interchange the sum and the angular integral. This interchange is valid because $1/(x - x_n)^{1/2}$ has an integrable singularity at $x = x_n$.

2.3. Limiting Cases

The oscillatory behaviors of $\langle \sigma_B^{(\text{abs})}(E_\nu) \rangle$ in Figs. 1 and 2 can be demonstrated analytically. Using the Poisson summation formula (see e.g., Ziman 1979):

$$\sum_{n=0}^{\infty} f\left(n + \frac{1}{2}\right) = \sum_{s=-\infty}^{\infty} (-1)^s \int_0^{\infty} f(x) e^{2\pi i s x} dx, \quad (15)$$

we can rewrite the sum in Eq. (14) as

$$\begin{aligned} & m_e^2 b \sum_n g_n \left[E_e^2 - m_e^2(1 + 2nb) \right]^{1/2} \\ &= \frac{2}{3} (E_e^2 - m_e^2)^{3/2} + (2m_e^2 b)^{3/2} \text{Re} \sum_{s=1}^{\infty} \frac{1-i}{4\pi i s^{3/2}} \exp \left[2\pi i s \left(\frac{E_e^2 - m_e^2}{2m_e^2 b} \right) \right]. \end{aligned} \quad (16)$$

The first term on the right-hand side of Eq. (16) corresponds to the zero-field result, and the second term (involving the sum of many oscillatory terms) corresponds to the correction due to the quantization effect. The sum is clearly convergent, and thus for small B , the averaged cross section $\langle \sigma_B^{(\text{abs})}(E_\nu) \rangle$ is reduced to the zero-field value $\langle \sigma_{B=0}^{(\text{abs})}(E_\nu) \rangle$.

For sufficiently large B at a given E_ν , or, equivalently, for sufficiently small E_ν at a given B , only the ground state Landau level is filled by the electron, i.e., $n_{\text{max}} = 0$ (see Eq. [8]). In this limit, $\langle \sigma_B^{(\text{abs})}(E_\nu) \rangle > \langle \sigma_{B=0}^{(\text{abs})}(E_\nu) \rangle / 4$, and only the first term in Eq. (7) needs to be retained. We then have

$$\langle \sigma_B^{(\text{abs})}(E_\nu) \rangle \simeq A \frac{m_e^2 b}{2\pi^2} \frac{(E_\nu + Q)}{[(E_\nu + Q)^2 - m_e^2]^{1/2}} (1 - f_e) \quad (17)$$

for ν_e absorption. A similar expression for $\bar{\nu}_e$ absorption is obtained by replacing Q with $-Q$ and μ_e with $-\mu_e$ in Eq. (17).

2.4. Discussion

The physical conditions which Figs. 1 and 2 are based on ($T = 3$ MeV, $Y_e = 0.1$, and $\mu_e = 20$ MeV, corresponding to a matter density of $\rho = 7.2 \times 10^{11}$ g cm $^{-3}$) are typical of the neutrinosphere of the proto-neutron star. In Fig. 3 we plot the ν_e and $\bar{\nu}_e$ absorption cross sections for a number of slightly different physical parameters, specified by b , μ_e and T (all with $Y_e = 0.1$). The cross section for elastic neutral-current scattering $\nu + N \rightarrow \nu + N$, $\sigma^{(\text{sc})}(E_\nu) \simeq G_F^2 E_\nu^2 / \pi$ (e.g., Tubbs & Schramm 1975), is also shown for comparison. Absorption dominates the transport of ν_e for high energies, with the ratio of absorption to scattering cross section per nucleon $(1 - Y_e) \sigma^{(\text{abs})} / \sigma^{(\text{sc})}$ approaching 5 for $E_\nu \gg \mu_e$. For smaller energies ($E_\nu \lesssim \mu_e$), absorption is severely suppressed by the Pauli blocking of the final electron states, and scattering becomes more important. In the case of $\bar{\nu}_e$, Pauli blocking is negligible, and scattering almost always dominates the transport, with the ratio of scattering to absorption cross section per nucleon $\sigma^{(\text{sc})} / [Y_e \sigma^{(\text{abs})}] \simeq 2(0.1/Y_e)$ for $E_\nu \gtrsim 10$ MeV.

As we can see from Figs. 1-3, for a given set of physical parameters of the medium (T , Y_e , μ_e or ρ), the magnetic field effect on the absorption opacity is more prominent for lower-energy neutrinos than for higher-energy ones. This is because for a given field strength, as the neutrino energy increases, more and more Landau levels become available for the electron in the final state (See Eq. [8]). Consequently, the electron phase space and hence the cross section should approach the zero-field values according to the correspondence principle. We found that typically when the number of Landau levels filled by the electron (n_{\max}) is greater than 2–3, the magnetic field effect on the absorption opacity becomes negligible. The “critical” neutrino energy is approximately given by

$$E_\nu^{(\text{crit})} \simeq m_e (2bn_{\max} + 1)^{1/2} \simeq 6 \left(\frac{n_{\max}}{3} \right)^{1/2} \left(\frac{B}{10^{15} \text{ G}} \right)^{1/2} \text{ MeV}. \quad (18)$$

For $E_\nu \gtrsim E_\nu^{(\text{crit})}$, one can approximate $\langle \sigma_B^{(\text{abs})}(E_\nu) \rangle$ by the zero-field value $\langle \sigma_{B=0}^{(\text{abs})}(E_\nu) \rangle$ with good accuracy (within a few percent). Alternatively, we can define a threshold magnetic field, B_{th} , above which the ν_e and $\bar{\nu}_e$ absorption opacities are modified (by more than a few percent) by the magnetic field:

$$B_{\text{th}} \simeq \frac{\langle E_\nu \rangle^2}{2n_{\max} m_e^2} B_c \simeq 3 \times 10^{15} \left(\frac{\langle E_\nu \rangle}{10 \text{ MeV}} \right)^2 \left(\frac{3}{n_{\max}} \right) \text{ G}, \quad (19)$$

where $\langle E_\nu \rangle \sim 10 \text{ MeV}$ is the average neutrino energy.

In the deeper layers of the neutron star, the typical neutrino energy is higher. Therefore we expect the magnetic field effect on the absorption opacities to be smaller there. In addition, for ν_e , absorption becomes unimportant as compared to scattering in the high density region (although not necessarily in the deepest interior, where ν_e can be degenerate). Thus, in order to assess the importance of the magnetic field effect on the neutrino emission, we only need to focus on the surface region, the region between the neutrinosphere and the neutrino-matter decoupling layer. We note that because the absorption opacities in the magnetic field for different neutrino energies oscillate around the the zero-field values, without a detailed calculation of the mean opacity (appropriately averaged over the neutrino energy spectrum) one cannot even answer the qualitative question such as whether the magnetic field increases or decreases the local neutrino energy flux.

In §§3–6, we study how the modified absorption cross sections affect the emergent ν_e and $\bar{\nu}_e$ energy fluxes and spectra from the proto-neutron star.

3. Neutrino Transport Near the Stellar Surface

As discussed in §2.4, the quantization effect of magnetic fields on neutrino absorption is important in the region only near the neutron star surface (between the neutrinosphere and the neutrino-matter decoupling layer). In this section we consider neutrino transport in this relatively low density region.

Because ν_e and $\bar{\nu}_e$ with typical energies of 10 MeV have comparable absorption and scattering opacities (see Fig. 3), the emergent ν_e and $\bar{\nu}_e$ energy fluxes and spectra are determined essentially in the same region where these two neutrino species just begin to thermally decouple from the proto-neutron star matter. The ν_e and $\bar{\nu}_e$ occupation numbers in this region are then approximately given by

$$f_{\nu_e}(E_\nu) = \frac{1}{\exp[(E_\nu/T) - \eta_\nu] + 1}, \quad (20)$$

and

$$f_{\bar{\nu}_e}(E_\nu) = \frac{1}{\exp[(E_\nu/T) + \eta_\nu] + 1}, \quad (21)$$

respectively, where $\eta_\nu = \mu_\nu/T$, and μ_ν is the ν_e chemical potential. From these occupation numbers, we obtain

$$n_{\nu_e} - n_{\bar{\nu}_e} = \frac{\eta_\nu}{6} \left(1 + \frac{\eta_\nu^2}{\pi^2} \right) T^3, \quad (22)$$

and

$$U_{\nu_e} + U_{\bar{\nu}_e} = \frac{7\pi^2}{120} \left(1 + \frac{30\eta_\nu^2}{7\pi^2} + \frac{15\eta_\nu^4}{7\pi^4} \right) T^4, \quad (23)$$

where for example, n_{ν_e} and U_{ν_e} are the number and energy densities, respectively, for the ν_e . We can estimate the magnitude of η_ν as follows. The net deleptonization rate of the proto-neutron star is

$$-\dot{N}_e \sim \frac{Y_{e,i}M/m_N}{t_{\text{diff}}} \sim c(n_{\nu_e} - n_{\bar{\nu}_e})\pi R^2, \quad (24)$$

where $Y_{e,i}$ is the initial electron fraction of the proto-neutron star, M is the proto-neutron star mass, m_N is the nucleon mass, t_{diff} is the neutrino diffusion timescale, and R is the proto-neutron star radius. The sum of the ν_e and $\bar{\nu}_e$ luminosities is

$$L_{\nu_e} + L_{\bar{\nu}_e} \sim \frac{1}{3} \frac{GM^2/R}{t_{\text{diff}}} \sim c(U_{\nu_e} + U_{\bar{\nu}_e})\pi R^2. \quad (25)$$

From Eqs. (22)–(25), we have

$$\eta_\nu \sim \frac{21\pi^2}{20} \frac{1 + (30/7\pi^2)\eta_\nu^2 + (15/7\pi^4)\eta_\nu^4}{1 + (\eta_\nu^2/\pi^2)} \frac{Y_{e,i}TR}{GMm_N} \sim 0.1 \left(\frac{Y_{e,i}}{0.36} \right) \left(\frac{T}{5 \text{ MeV}} \right) \ll 1, \quad (26)$$

where the numerical value is obtained for $M \simeq 1.4M_\odot$ and $R \simeq 10$ km. Therefore, to a good approximation, the ν_e and $\bar{\nu}_e$ in the decoupling region have Fermi-Dirac energy distributions with zero chemical potentials.

Let $I_E = I_E(\mathbf{r}, \hat{\Omega})$ be the specific intensity of neutrinos of a given species, where \mathbf{r} is the spatial position, and $\hat{\Omega}$ specifies the direction of propagation. The general transport equation takes the form

$$\hat{\Omega} \cdot \nabla I_E = \rho \kappa_E^{(\text{abs})^*} I_E^{(FD)} + \rho \kappa_E^{(\text{sc})} \frac{1}{4\pi} \int d\Omega' I'_E - \rho \left[\kappa_E^{(\text{abs})^*} + \kappa_E^{(\text{sc})} \right] I_E, \quad (27)$$

where $I'_E = I_E(\mathbf{r}, \hat{\Omega}')$, and the subscript “ E ” indicates that the relevant physical quantities depend on the neutrino energy E . The opacities $\kappa_E^{(\text{abs})^*}$ and $\kappa_E^{(\text{sc})}$ are related to the corresponding cross sections as, e.g., $\kappa_E^{(\text{abs})^*} = (1 - Y_e)\sigma_E^{(\text{abs})^*}/m_N$ and $\kappa_E^{(\text{sc})} = \sigma_E^{(\text{sc})}/m_N$ for ν_e . Note that we have included the effect of stimulated absorption for neutrinos (e.g., Imshennik & Nadezhin 1973) by introducing the corrected absorption opacity $\kappa_E^{(\text{abs})^*} = \kappa_E^{(\text{abs})}[1 + \exp(-E/T)]$ (T is the matter temperature). Hereafter, we shall suppress the superscript “ $*$ ” in $\kappa_E^{(\text{abs})^*}$, and the notation $\kappa_E^{(\text{abs})}$ should be understood as having included the correction due to stimulated absorption. The quantity $I_E^{(FD)}$ in Eq. (27) is the equilibrium neutrino intensity, given by the Fermi-Dirac distribution

$$I_E^{(FD)} = \frac{E^3}{c^2 h^3} \frac{1}{\exp(E/T) + 1}. \quad (28)$$

Note that the time derivative term ($\partial I_E/\partial t$) on the left-hand-side of Eq. (27) has been neglected. This corresponds to an instantaneous redistribution of emission and absorption sources (i.e., an instantaneous redistribution of matter temperature) — The timescale for the redistribution is of order the mean free path divided by c , much smaller than the neutrino cooling time of the star.

The zeroth order moment of the transport equation can be written as

$$\nabla \cdot \mathbf{F}_E = \rho \kappa_E^{(\text{abs})} c (U_E^{(FD)} - U_E), \quad (29)$$

where $\mathbf{F}_E = \int I_E \hat{\Omega} d\Omega$ is the (spectral) neutrino energy flux, $U_E = \int I_E d\Omega/c$ is the energy density, and $U_E^{(FD)} = (4\pi/c)I_E^{(FD)}$ is the corresponding equilibrium energy density. With the Eddington closure relation, the first moment of Eq. (27) becomes

$$\mathbf{F}_E = -\frac{c}{3\rho\kappa_E^{(t)}} \nabla U_E, \quad (30)$$

where $\kappa_E^{(t)} = \kappa_E^{(\text{abs})} + \kappa_E^{(\text{sc})}$. Equations (29) and (30) completely specify the neutrino radiation field.

4. Rosseland Mean Opacities

Here we are concerned with the total neutrino energy flux emitted from a local surface region of the neutron star. The magnetic field strength in this local region is assumed to be constant. Since the scale heights for physical quantities such as the matter density and temperature are much smaller than the local radii, we adopt the plane-parallel geometry. Integrating Eq. (30) over the neutrino energy, we find that the total neutrino energy flux (of a specific species) $\mathbf{F} = \int \mathbf{F}_E dE = F \hat{\mathbf{r}}$ is given by

$$F = -\frac{c}{3\rho\kappa_R} \frac{dU}{dr}, \quad (31)$$

where $U = \int U_E dE$ is the total neutrino energy density, and κ_R is the “Rosseland mean opacity” defined as

$$\frac{1}{\kappa_R} = \frac{\int dE (1/\kappa_E^{(t)}) (dU_E/dr)}{\int dE (dU_E/dr)}. \quad (32)$$

Since neutrino emission and absorption rates are extremely fast even in the regions near the proto-neutron star surface, a radiative equilibrium⁴ approximately holds, i.e.,

$$\int \rho \kappa_E^{(\text{abs})} (U_E^{(FD)} - U_E) dE \simeq 0. \quad (33)$$

From Eq. (29), we have $dF/dr \simeq 0$, or F is approximately constant.

If we introduce the Rosseland mean optical depth measured from the stellar surface via $d\tau_R = -\rho \kappa_R dr$, with F constant, Eq. (31) can be integrated to yield

$$cU = 3F \left(\tau_R + \frac{2}{3} \right), \quad (34)$$

where we have used the boundary condition $F = cU/2$ at the surface ($\tau_R = 0$). Equation (34) resembles the standard Eddington profile. Note that outside the decoupling region the neutrino energy density U may not be equal to $U^{(FD)} = (7\pi^4/240)T^4$ specified by the matter temperature T . Similarly, U_E may differ substantially from $U_E^{(FD)}(T)$ (see §6). However, we can still approximate U_E by the Fermi-Dirac function at the neutrino temperature T_ν , which is equal to the matter temperature at the decoupling layer. Equation (32) can then be rewritten as

$$\frac{1}{\kappa_R} = \frac{30}{7\pi^4 T_\nu^5} \int dE \frac{1}{\kappa_E^{(t)}} \frac{E^4 \exp(E/T_\nu)}{[\exp(E/T_\nu) + 1]^2}. \quad (35)$$

With the cross sections given in §2, we can calculate the Rosseland mean opacity $\kappa_R(B)$ in magnetic fields using Eq. (35). Note that in Eq. (35) $\kappa_E^{(t)}$ depends on the local matter temperature T . Only in the regions not far from the decoupling layer, do we have $T_\nu = T$.

Figure 4 shows the ratio of the Rosseland mean opacity $\kappa_R(B)$ of ν_e to the zero-field value $\kappa_R(0)$ as a function of the magnetic field strength for typical conditions near the proto-neutron star surface. We choose these conditions to be $T = T_\nu = 3, 5$ MeV, and $\mu_e = 10, 15, 20$ MeV, all with $Y_e = 0.1$. Figure 5 shows similar results for $\bar{\nu}_e$ with similar physical parameters ($T = T_\nu = 3, 5, 7$ MeV; Note that the results are insensitive to μ_e). We see that deviation of $\kappa_R(B)$ from the zero-field value by more than 5% generally requires field strength $b = B/B_c \gtrsim 100$.

The behavior of the ratio $\kappa_R(B)/\kappa_R(0)$ as a function of b is certainly not obvious a priori. Since the Rosseland mean integral is dominated by neutrinos with the smallest opacities, and since $\kappa_B^{(\text{abs})}$ scales linearly with B in the regime where only the ground Landau level is filled (see Eq. [17]), we expect that for sufficiently large B , the Rosseland mean opacity increases linearly with increasing B . This is indeed what is indicated in Figs. 4 and 5. For “intermediate” field

⁴In principle, the overall radiative equilibrium involves matter and neutrinos of all species. However, because the coupling between matter and $\nu_\mu, \bar{\nu}_\mu, \nu_\tau,$ and $\bar{\nu}_\tau$ is much weaker, the overall radiative equilibrium in the region near the proto-neutron star surface mainly involves matter and ν_e and $\bar{\nu}_e$. Since the coupling between matter and ν_e is comparable to that between matter and $\bar{\nu}_e$, we further assume that an approximate radiative equilibrium holds separately for ν_e and $\bar{\nu}_e$.

strength, the $\kappa_B^{(\text{abs})}$ curve for ν_e (see Fig. 1) has a significant portion which is below the zero-field value at low neutrino energies. For such intermediate fields, we would expect $\kappa_R(B)$ to be less than the zero-field value. This explains the non-monotonic behavior of $\kappa_R(B)/\kappa_R(0)$ as a function of B shown in Fig. 4. For $\bar{\nu}_e$, the non-monotonic behavior is much less pronounced (see the curve for $T = 7$ MeV in Fig. 5) since the energy range in which $\kappa_B^{(\text{abs})} < \kappa_{B=0}^{(\text{abs})}$ is smaller.

5. Differential Neutrino Fluxes and Neutron Star Kick From Asymmetric Magnetic Field Topology

Imagine a proto-neutron star with an asymmetric magnetic field topology, e.g., the north pole and the south pole have different *magnitudes* of magnetic field (say, by a factor of a few). What is the difference in the neutrino fluxes from these two regions due to the different absorption opacities of ν_e and $\bar{\nu}_e$, and what is the resulting kick velocity of the neutron star? We recall that the fractional asymmetry α in the total neutrino emission (of all species) required to generate a kick velocity V_{kick} is $\alpha = 0.028 [V_{\text{kick}}/(10^3 \text{ km s}^{-1})] [E_{\text{tot}}/(3 \times 10^{53} \text{ erg})]$, where E_{tot} is the total neutrino energy radiated from the neutron star (the neutron star mass has been set to $1.4 M_\odot$).

To quantitatively understand how the magnetically-modified opacities change the local neutrino flux, we will have to evaluate these opacities at different depths (corresponding to different physical conditions) below the neutron star surface, and to perform complete cooling calculations which take into account these opacities. However, Figs. 4 and 5 clearly indicate that, even near the stellar surface, where one expects the modification to the opacities to be most prominent, and even with the most favorable conditions for the magnetic field to be effective in changing the opacities (i.e., low density and low temperature), a 5% change in the Rosseland mean opacity (for ν_e or $\bar{\nu}_e$) requires a magnetic field with $b \gtrsim 100$, or $B \gtrsim 4 \times 10^{15}$ G. In the following, we shall content ourselves with merely estimating the change in the local neutrino flux from the modified opacities.

We first consider the case in which the matter temperature throughout the neutron star is unaffected by the magnetic field. One might imagine this as a possibility if convection dominates energy transfer between different parts of the star. Under the neutrino-matter decoupling layer the specific neutrino energy density U_E is the same as the Fermi-Dirac function $U_E^{(FD)}(T)$ specified by the matter temperature. The emergent neutrino flux is then inversely proportional to the Rosseland mean optical depth τ_R from the decoupling layer to the stellar surface (see Eq. [34]). Since τ_R for ν_e or $\bar{\nu}_e$ at the decoupling layer is of order a few, the flux F is inversely proportional to κ_R evaluated near the decoupling region. If we use the curve for $T = 3$ MeV and $\mu_e = 10$ MeV in Fig. 4 (which has the most pronounced magnetic correction), we find that the fractional change in the ν_e flux is $\delta F_{\nu_e}/F_{\nu_e} \sim 0.1$ at $b = 100$ (If we used the curve for $\mu_e = 15$ or 20 MeV, which more closely represents the physical condition at the decoupling region, the modification $\delta F_{\nu_e}/F_{\nu_e}$ would be smaller by a factor of a few or more). Similarly, using the curve for $T = 3$ MeV in Fig. 5 to maximize the magnetic correction, we find $\delta F_{\bar{\nu}_e}/F_{\bar{\nu}_e} \sim -0.02$ at $b = 100$. Since the fluxes of

other types of neutrinos are unchanged⁵, and since different neutrino species more or less carry away the same amount of energy, the change in the total neutrino flux is only $\delta F_{\text{tot}}/F_{\text{tot}} \sim 0.01$ at $b = 100$. If we now imagine that the north pole of the neutron star has $b \sim 100$ while the south pole has a field strength a factor of a few smaller, then, taking into account the geometric reduction ($\sim 1/3$), the flux asymmetry is about $\alpha \sim 0.003$, just enough to give a kick velocity of $\sim 100 \text{ km s}^{-1}$ to the neutron star. With κ_R evaluated at more realistic conditions, we expect the resulting α to be even smaller.

The assumption that the matter temperature is unaffected by the magnetic field (and therefore spherically symmetric) is unlikely to be valid. In reality, when a region of the star (say the north pole) emits more flux, it also cools faster. With reduced temperature, this region will tend to emit less flux. In the extreme case, one would find $F \sim cU_0/\tau_R$, with U_0 the neutrino energy density in the stellar core, and τ_R the Rosseland mean optical depth from the core to the surface. Since in the bulk interior of the star, modification to κ_R due to the magnetic field is negligible, we would conclude that the change in the neutrino flux is much smaller than what is estimated in the last paragraph.

To summarize, the modifications to the absorption opacities of ν_e and $\bar{\nu}_e$ due to quantized Landau levels give rise to rather small change in neutrino fluxes from the neutron star. To generate appreciable kick velocities ($\sim 300 \text{ km s}^{-1}$) from this effect requires the difference of field strengths at the two opposite poles to be at least 10^{16} G (and possibly much larger).

6. Magnetic Field Effect on ν_e and $\bar{\nu}_e$ Energy Spectra

We now consider how the oscillatory behaviors (see Figs. 1–3) of the absorption opacities of ν_e and $\bar{\nu}_e$ may manifest themselves in the radiated neutrino energy spectra. For an absorption dominated medium, neutrinos with energy E decouple from the matter and start free-streaming at a column depth (in g cm^{-2}) $y = \int \rho dr \sim 1/\kappa_E^{(\text{abs})}$. Thus the neutrino energy spectrum is given by $F_E \sim cU_E^{(FD)}$ with $U_E^{(FD)}$ evaluated at the depth $y \sim 1/\kappa_E^{(\text{abs})}$. In the presence of significant scattering, decoupling occurs at depth $y \sim 1/\kappa_E^{\text{eff}}$ with the effective opacity $\kappa_E^{\text{eff}} \sim \sqrt{\kappa_E^{(\text{abs})} \kappa_E^{(t)}}$, whereas the neutrinosphere from which neutrinos start free-streaming is located at $y \sim 1/\kappa_E^{(t)}$. Near the decoupling region we have $dU_E/dr \sim -\rho \kappa_E^{\text{eff}} U_E^{(FD)}$, and thus from Eq. (30) the neutrino spectral energy flux is given by

$$F_E \sim \frac{\kappa_E^{\text{eff}}}{\kappa_E^{(t)}} cU_E^{(FD)}(y \sim 1/\kappa_E^{\text{eff}}). \quad (36)$$

⁵The decoupling layers of $\nu_{\mu(\tau)}$ and $\bar{\nu}_{\mu(\tau)}$ depend on the ν - e scattering cross sections, which can be affected by the magnetic field. However, the layers are located much deeper than those of ν_e and $\bar{\nu}_e$ (since ν - e scattering opacity is small), the modification to the ν - e scattering opacity due to electron Landau levels is therefore smaller than the modification to the absorption opacities of ν_e and $\bar{\nu}_e$ considered in this paper.

The above qualitative argument can be made more rigorous by directly solving Eqs. (29) and (30). Consider a plane-parallel atmosphere and define the (energy-dependent) optical depth via $d\tau_E = -\rho\kappa_E^{(t)} dr = \kappa_E^{(t)} dy$. Equations (29) and (30) can be combined to give

$$\frac{d^2}{d\tau_E^2} U_E = \beta_E^2 [U_E - U_E^{(FD)}], \quad \text{with} \quad \beta_E^2 = 3 \frac{\kappa_E^{(\text{abs})}}{\kappa_E^{(t)}}. \quad (37)$$

With a constant β_E , the above equation can be solved exactly. For the boundary condition $F_E = (c/3)(dU_E/d\tau_E) = cU_E/2$ at $\tau_E = 0$, the neutrino energy flux at the surface is given by

$$F_E = \frac{\beta_E/3}{1 + 2\beta_E/3} \int_0^\infty d\tau_E \beta_E c U_E^{(FD)}(\tau_E) \exp(-\beta_E \tau_E) \simeq \frac{\beta_E/3}{1 + 2\beta_E/3} c U_E^{(FD)}(\tau_E \simeq \beta_E^{-1}). \quad (38)$$

Figure 6 shows the spectral energy fluxes of ν_e calculated using Eq. (38) for different field strengths ($b = 100$ and 300). The matter temperature profile is obtained from Eq. (34) assuming $U \propto T^4$. For a total energy flux of $F = (c/4)U(T_{\text{eff}})$ (where T_{eff} is the effective temperature), we have $T = T_{\text{eff}}[(3/4)\tau_R + 1/2]^{1/4}$. We choose $T_{\text{eff}} = 3$ MeV in these examples. For simplicity, we have neglected the variations of the opacities as a function of τ_E . Thus the temperature at decoupling ($\tau_E \simeq \beta_E^{-1}$; see Eq. [38]) is given by $T \simeq T_{\text{eff}}[(3/4)\kappa_R/\kappa_E^{(\text{eff})} + 1/2]^{1/4}$, where $\kappa_E^{(\text{eff})} = \beta_E \kappa_E^{(t)} = \sqrt{3\kappa_E^{(\text{abs})}\kappa_E^{(t)}}$ and we take the relevant opacities to have the corresponding values for $Y_e = 0.1$, $\mu_e = 20$ MeV, and $T = 3$ MeV. This simplification should not introduce qualitative changes in the spectrum. As seen from Fig. 6, the spectrum is pinched at the high energies because of the E^2 -dependence of the opacities. The magnetic field introduces modulations in the spectrum. For lower magnetic field strengths, the modulations occur at the lower energy band. As the magnetic field gets stronger, the modulations shift to the higher energy part of the spectrum.

The distortions and modulations of the ν_e and $\bar{\nu}_e$ energy spectra by strong magnetic fields may offer an interesting possibility to limit the magnetic field strength in proto-neutron stars through the detection of neutrinos from a Galactic supernova. We note, however, that the ν_e spectra shown in Fig. 6 are based on very approximate calculations. They serve only as illustrative examples of the magnetic field effect on the neutrino spectra. More detailed calculations are needed to obtain realistic spectra which include the magnetic field effect.

7. Conclusion

In this paper, we have studied the issue of whether asymmetric magnetic field topology in a proto-neutron star can induce asymmetric neutrino emission from the star through the modifications of the neutrino absorption opacities by the magnetic field. These modifications arise from the quantized Landau levels of electrons and positrons produced in strong magnetic fields. By calculating the appropriate mean neutrino opacities in the magnetic field, we demonstrate that this mechanism is rather inefficient in generating a kick to the neutron star: To obtain appreciable

kick velocities ($\sim 300 \text{ km s}^{-1}$), the difference in the field strengths at the two opposite poles of the star must be at least 10^{16} G .

This work was started while D.L. held the Richard C. Tolman postdoctoral Fellowship at Caltech. Additional support was provided by NASA grant NAG 5-2756 and NSF grant AST-9417371, as well as a start-up fund for new faculty at Cornell University. Y.Q. is supported by the David W. Morrisroe postdoctoral Fellowship at Caltech.

REFERENCES

- Akhmedov, E. K., Lanza, A., & Sciama, D. W. 1997, *Phys. Rev. D*, 56, 6117.
- Arras, P., & Lai, D. 1998, submitted to *Phys. Rev. Lett.*
- Arzoumanian, Z., Phillips, J. A., Taylor, J. H., & Wolszczan, A. 1996, *ApJ*, 470, 1111.
- Aschenbach, B., Egger, R., & Trumper, J. 1995, *Nature*, 373, 587.
- Bazan, G., & Arnett, D. 1994, *ApJ*, 433, L41.
- Bezchastnov, V. G., & Haensel, P. 1996, *Phys. Rev. D*, 54, 3706.
- Bisnovatyi-Kogan, G. S. 1993, *Astron. Astrophys. Trans.*, 3, 287.
- Brandt, N., & Podsiadlowski, P. 1995, *MNRAS*, 274, 461.
- Burrows, A., & Fryxell, B. A. 1992, *Science*, 258, 430.
- Burrows, A., Hayes, J., & Fryxell, B. A. 1995, *ApJ*, 450, 830.
- Burrows, A., & Hayes, J. 1996, *Phys. Rev. Lett.*, 76, 352.
- Chugai, N. N. 1984, *Sov. Astron. Lett.*, 10, 87.
- Cordes, J. M., & Chernoff, D. F. 1997, *ApJ*, submitted (astro-ph/9707308).
- Cordes, J. M., Romani, R. W., & Lundgren, S. C. 1993, *Nature*, 362, 133.
- Cordes, J. M., Wasserman, I., & Blaskiewicz, M. 1990, *ApJ*, 349, 546.
- Cropper, et al. 1988, *MNRAS*, 231, 695.
- Dewey, R. J., & Cordes, J. M. 1987, *ApJ*, 321, 780.
- Dorofeev, O. F., et al. 1985, *Sov. Astron. Lett.*, 11, 123.
- Fassio-Canuto, L. 1969, *Phys. Rev.*, 187, 2141.

- Frail, D. A., Goss, W. M., & Whiteoak, J. B. Z. 1994, *ApJ*, 437, 781.
- Fryer, C., Burrows, A., & Benz, W. 1998, *ApJ*, in press (astro-ph/9710333)
- Fryer, C., & Kalogera, V. 1997, *ApJ*, in press (astro-ph/9706031).
- Goldreich, P., Lai, D., & Sahrting, M. 1996, in “Unsolved Problems in Astrophysics”, ed. J. N. Bahcall and J. P. Ostriker (Princeton University press).
- Gott, J. R., Gunn, J. E., & Ostriker, J. P. 1970, *ApJ*, 160, L91.
- Gunn, J. E., & Ostriker, J. P. 1970, *ApJ*, 160, 979.
- Hansen, B. M. S., & Phinney, E. S. 1997, *MNRAS*, 291, 569.
- Harrison, E. R., & Tademaru, E. 1975, *ApJ*, 201, 447.
- Harrison, P. A., Lyne, A. G., & Anderson, B. 1993, *MNRAS*, 261, 113.
- Herant, M., Benz, W., Hix, W. R., Fryer, C. L., & Colgate, S. A. 1994, *ApJ*, 435, 339.
- Horowitz, C. J., & Li, G. 1997, astro-ph/9705126.
- Horowitz, C. J., & Piekarewicz, J. 1997, hep-ph/9701214.
- Iben, I., & Tutukov, A. V. 1996, *ApJ*, 456, 738.
- Imshennik, V. S., & Nadezhin, D. K. 1973, *Sov. Phys. JETP*, 36, 821.
- Janka, H.-T., & Müller, E. 1994, *A&A*, 290, 496.
- Janka, H.-T., & Müller, E. 1996, *A&A*, 306, 167.
- Kaspi, V. M., et al. 1996, *Nature*, 381, 584.
- Kusenko, A., & Segré, G. 1996, *Phys. Rev. Lett.*, 77, 4872.
- Lai, D. 1996, *ApJ*, 466, L35.
- Lai, D., Bildsten, L., & Kaspi, V. M. 1995, *ApJ*, 452, 819.
- Lai, D., & Goldreich, P. 1998, in preparation.
- Lai, D., & Qian, Y.-Z. 1998, *ApJ*, 495, L103.
- Lorimer, D. R., Bailes, M., & Harrison, P. A. 1997, *MNRAS*, 289, 592.
- Lyne, A. G., & Lorimer, D. R. 1994, *Nature*, 369, 127.
- Matese, J. J., & O’Connell, R. F. 1969, *Phys. Rev.*, 180, 1289.

- McCray, R. 1993, *ARA&A*, 31, 175.
- Minkowski, R. 1970, *PASP*, 82, 470.
- Morse, J. A., Winkler, P. F., & Kirshner, R. P. 1995, *AJ*, 109, 2104.
- Qian, Y.-Z. 1997, *Phys. Rev. Lett.*, 79, 2750.
- Roulet, E. 1997, Preprint, hep-ph/9711206.
- Taylor, J. H., & Cordes, J. M. 1993, *ApJ*, 411, 674.
- Trammell, S. R., Hines, D. C., & Wheeler, J. C. 1993, *ApJ*, 414, L21.
- Tubbs, D. L., & Schramm, D. N. 1975, *ApJ*, 201, 467.
- Utrobin, V. P., Chugai, N. N., & Andronova, A. A. 1995, *A&A*, 295, 129.
- Vilenkin, A. 1995, *ApJ*, 451, 700.
- Ziman, J. M. 1979, *Principles of the Theory of Solids* (Cambridge Univ. Press: Cambridge), p. 319.

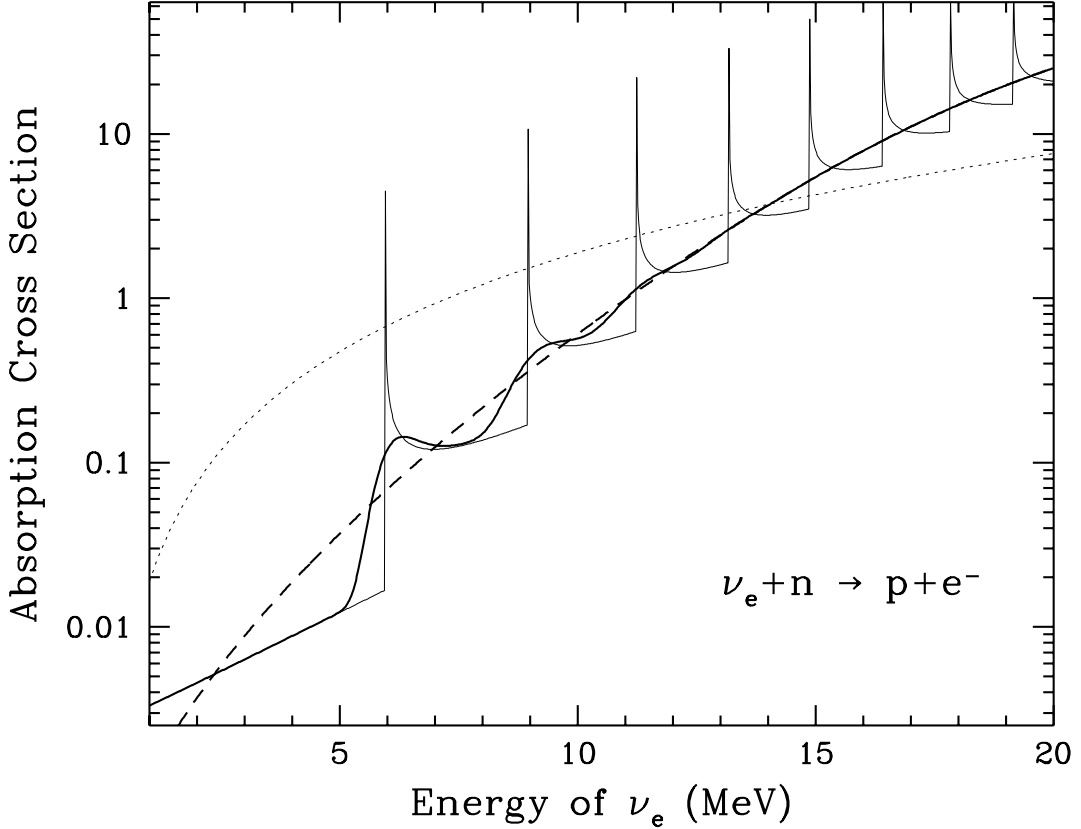


Fig. 1.— Absorption cross section (per nucleon) of ν_e , $(1 - Y_e)\sigma_B^{(\text{abs})}(E_\nu)$, in units of $A \times \text{MeV}^2 = \pi G_F^2 \cos^2 \theta_C (c_V^2 + 3c_A^2) \times \text{MeV}^2 \simeq 0.91 \times 10^{-42} \text{ cm}^2$, as a function of the neutrino energy. The dashed line is the zero-field result (The effect of the nucleon thermal motion is included but is hard to discern). The heavy and the light solid lines are the results for $b = 100$, with and without the effect of the nucleon thermal motion, respectively. The dotted line is the elastic scattering cross section, $\sigma^{(\text{sc})}(E_\nu)$, in the same units. All results are for $T = 3 \text{ MeV}$, $Y_e = 0.1$, and $\mu_e = 20 \text{ MeV}$ (corresponding to $\rho = 7.2 \times 10^{11} \text{ g cm}^{-3}$).

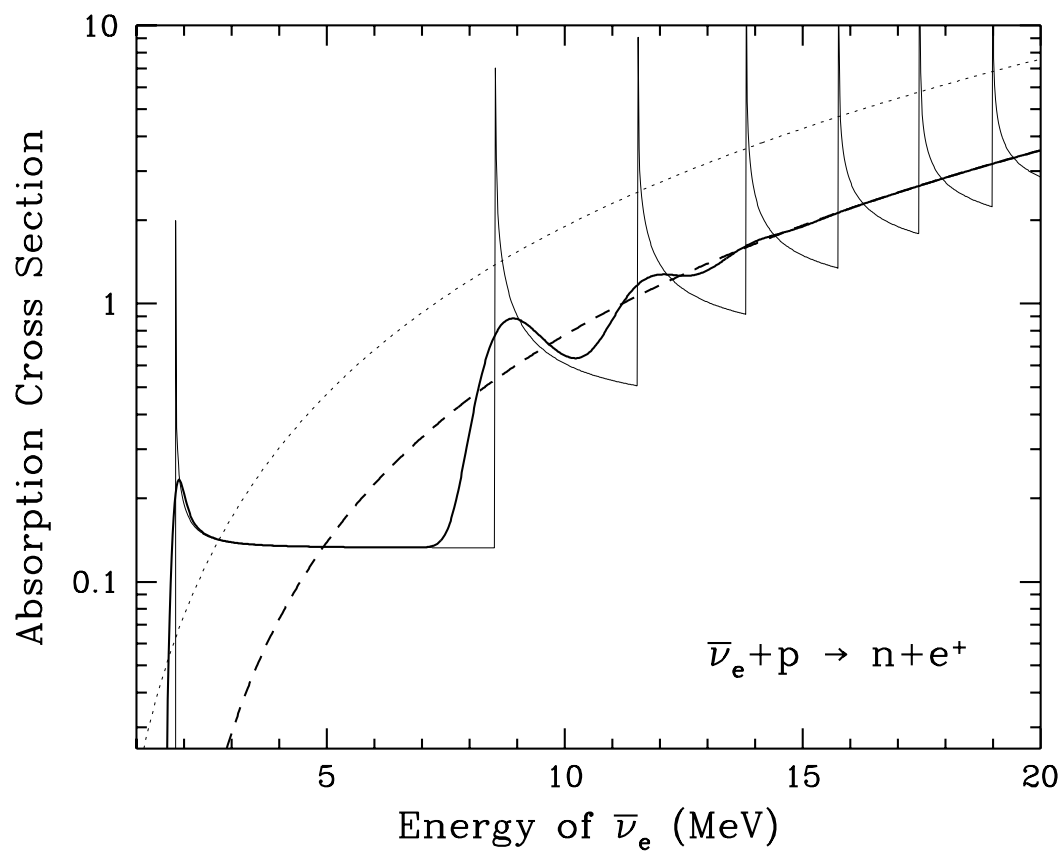


Fig. 2.— Absorption cross section (per nucleon) of $\bar{\nu}_e$, $Y_e \sigma_B^{(\text{abs})}(E_\nu)$. The physical parameters, units, and labels are the same as in Fig. 1.

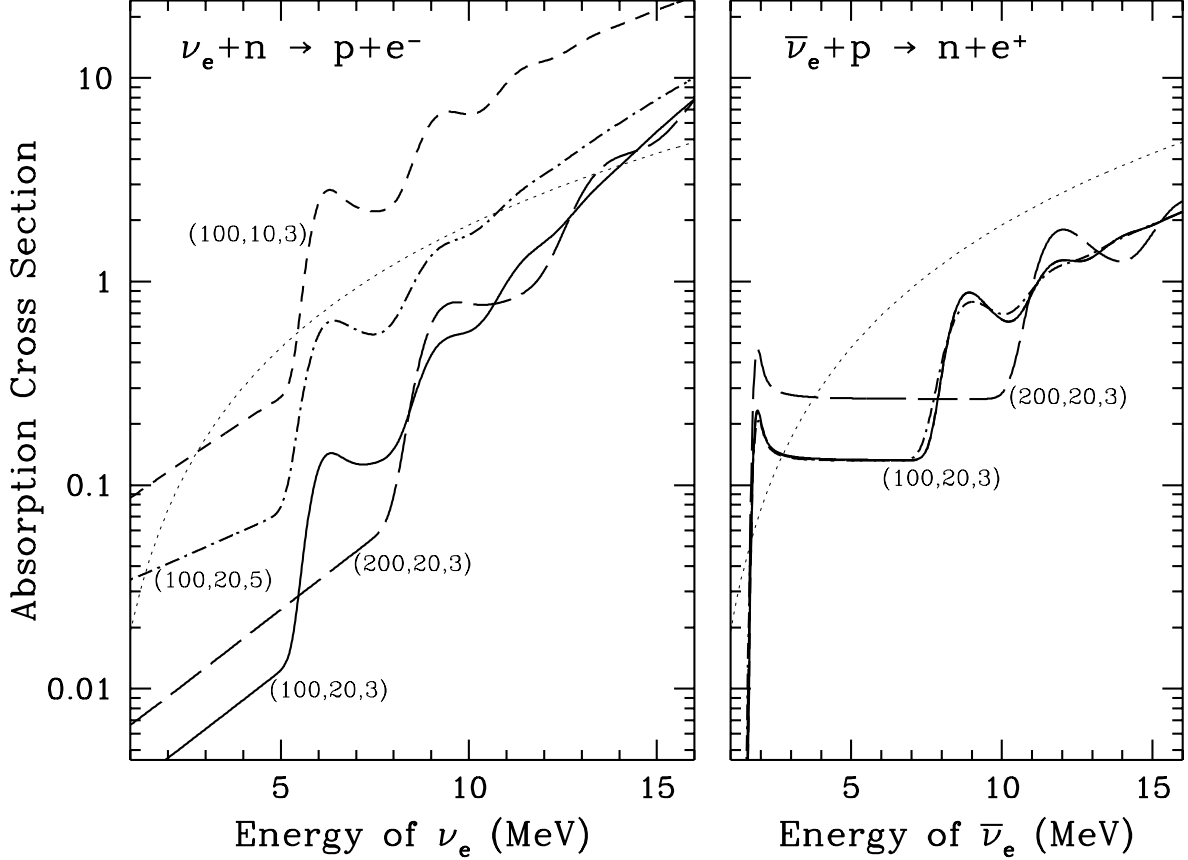


Fig. 3.— Absorption cross sections (per nucleon) of ν_e (left panel) and $\bar{\nu}_e$ (right panel), in units of $A \times \text{MeV}^2 = \pi G_F^2 \cos^2 \theta_C (c_V^2 + 3c_A^2) \times \text{MeV}^2 \simeq 0.91 \times 10^{-42} \text{ cm}^2$, as functions of the neutrino energy for different physical parameters. All results assume $Y_e = 0.1$. The solid, the short-dashed, the long-dashed, and the dot-dashed curves are for $(b, \mu_e/\text{MeV}, T/\text{MeV}) = (100, 20, 3)$, $(100, 10, 3)$, $(200, 20, 3)$, and $(100, 20, 5)$, respectively. [Note that for $\bar{\nu}_e$, the curve for $(b, \mu_e/\text{MeV}, T/\text{MeV}) = (100, 10, 3)$ is almost identical to the curve for $(b, \mu_e/\text{MeV}, T/\text{MeV}) = (100, 20, 3)$, and both curves are close to the curve for $(b, \mu_e/\text{MeV}, T/\text{MeV}) = (100, 20, 5)$.] The light dotted lines are the elastic scattering cross sections in the same units.

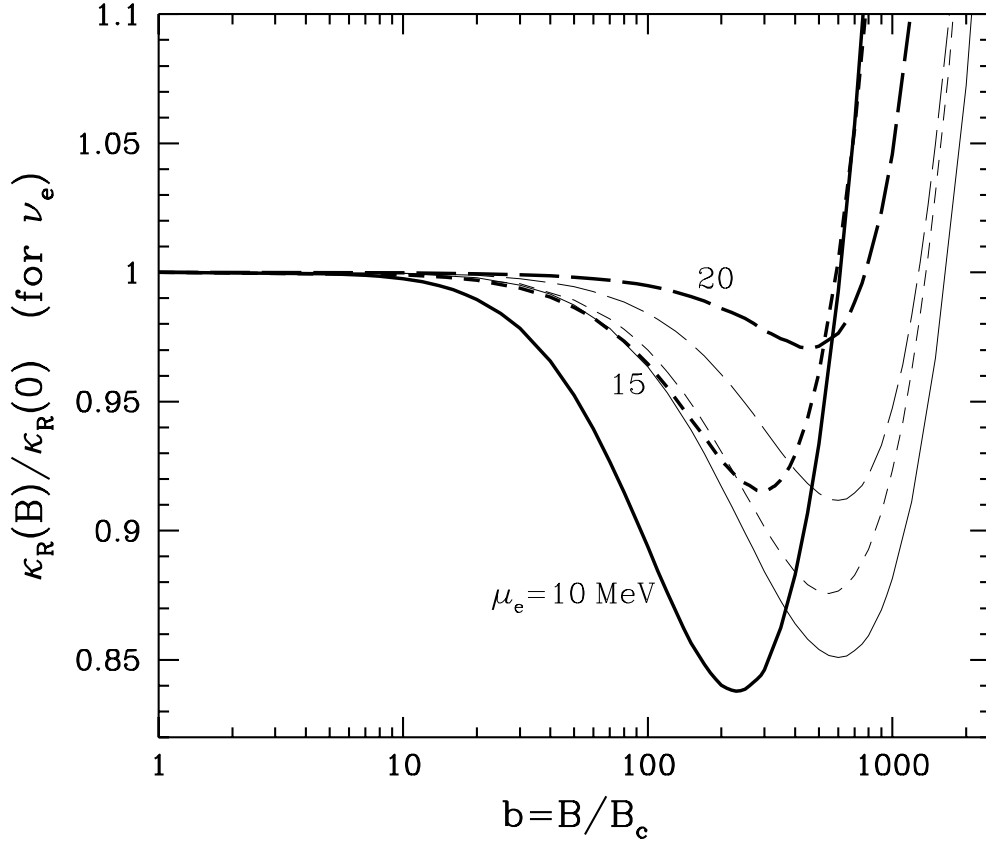


Fig. 4.— The ratio of the Rosseland mean opacity $\kappa_R(B)$ of ν_e to its zero-field value $\kappa_R(0)$ as a function of the magnetic field strength $b = B/B_c$ (with $B_c = 4.414 \times 10^{13}$ G). All results assume $Y_e = 0.1$. The heavier curves correspond to $T = T_\nu = 3$ MeV, and the lighter curves correspond to $T = T_\nu = 5$ MeV. The solid, the short-dashed, and the long-dashed lines are for $\mu_e = 10, 15,$ and 20 MeV, respectively.

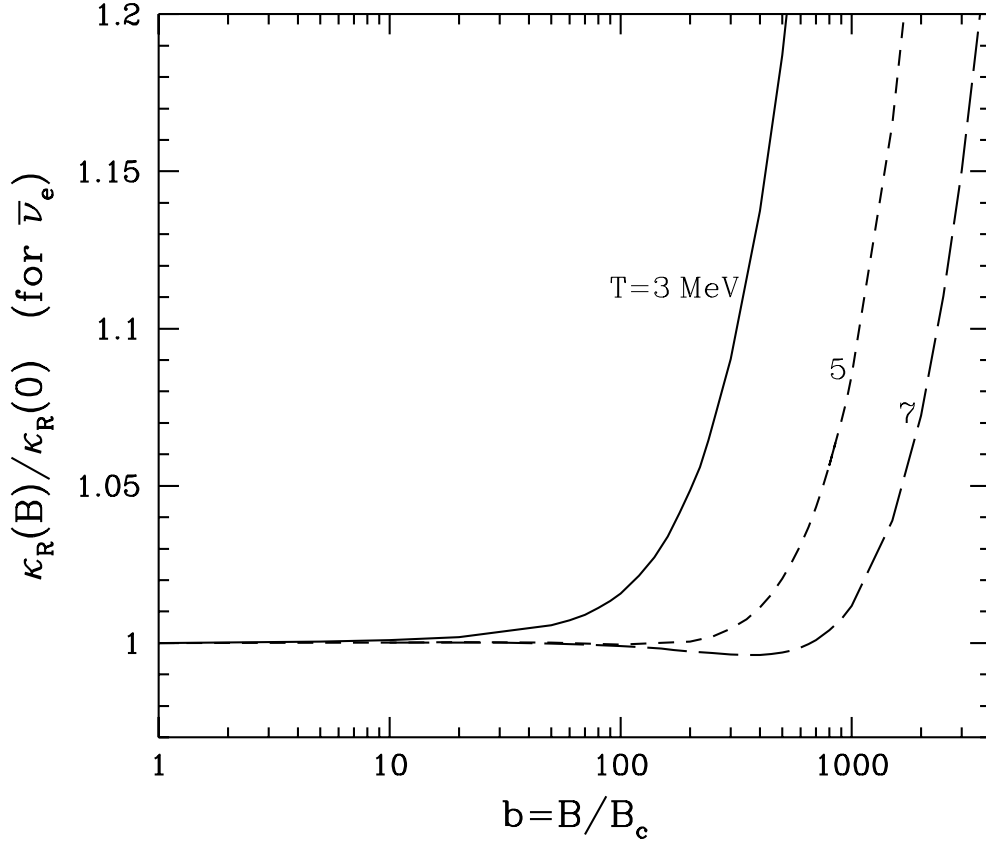


Fig. 5.— The ratio of the Rosseland mean opacity $\kappa_R(B)$ of $\bar{\nu}_e$ to its zero-field value $\kappa_R(0)$ as a function of the magnetic field strength $b = B/B_c$ (with $B_c = 4.414 \times 10^{13}$ G). All results assume $Y_e = 0.1$ and $\mu_e = 20$ MeV (but the results are rather insensitive to the value of μ_e). The solid, the short-dashed, and the long-dashed line are for $T = T_\nu = 3, 5,$ and 7 MeV, respectively. Note that the results mainly depend on T_ν , and are rather insensitive to T .

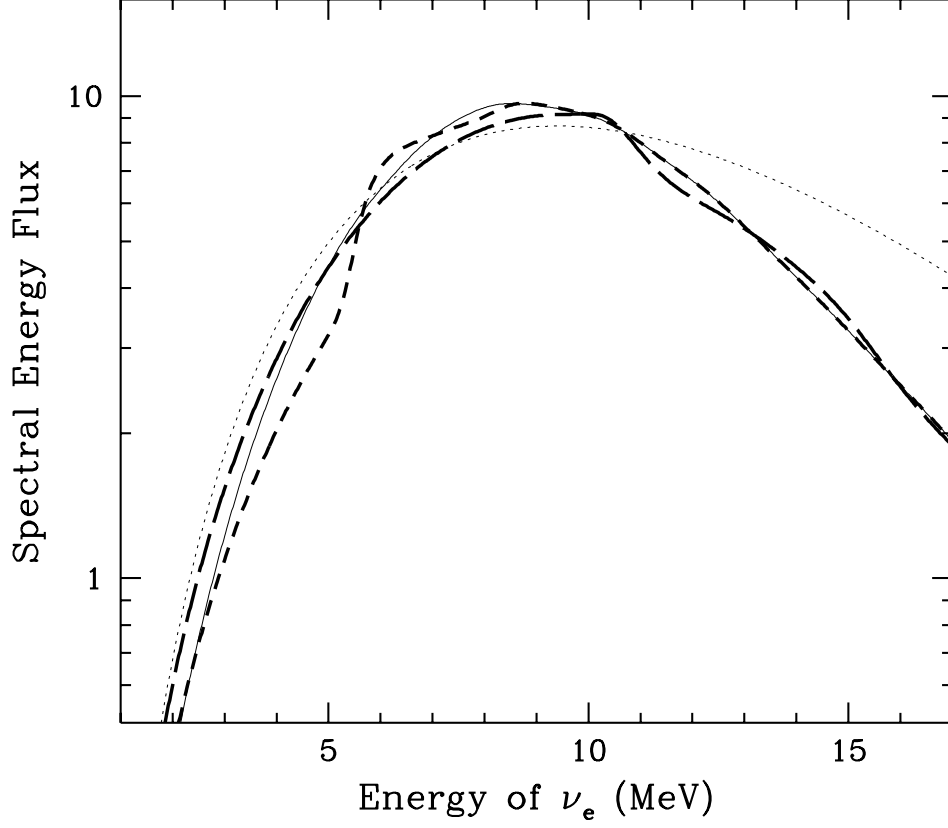


Fig. 6.— Illustrative examples of the ν_e spectral energy fluxes (in arbitrary units) modified by the magnetic fields. The light solid, the short-dashed, and the long-dashed line are for $b = 0, 100,$ and $300,$ respectively. The light dotted line is the Fermi-Dirac spectrum with $T = T_{\text{eff}} = 3$ MeV.